Neutrons from multiplicity-selected La-La and Nb-Nb collisions at 400*A* MeV and La-La collisions at 250*A* MeV

M. M. Htun,[1,*] R. Madey,[1] W. M. Zhang,[1] M. Elaasar,[1,†] D. Keane,[1] B. D. Anderson,[1] A. R. Baldwin,[1] J. Jiang,[1,‡] A. Scott,[1] Y. Shao,[1,§] J. W. Watson,[1] K. Frankel,[2] L. Heilbronn,[2] G. Krebs,[2] M. A. McMahan,[2] W. Rathbun,[2] J. Schambach,[2,‖] G. D. Westfall,[3] S. Yennello,[3,¶] C. Gale,[4] and J. Zhang[4]

[1]*Kent State University, Kent, Ohio 44242*

[2]*Lawrence Berkeley Laboratory, Berkeley, California 94720*

[3]*Michigan State University, East Lansing, Michigan 44828*

[4]*McGill University, Montréal, Québec, Canada H3A 2T8*

(Received 1 September 1998)

Triple-differential cross sections for neutrons from high-multiplicity La-La collisions at 250 and 400 MeV per nucleon and Nb-Nb collisions at 400 MeV per nucleon were measured at several polar angles as a function of the azimuthal angle with respect to the reaction plane of the collision. The reaction plane was determined by a transverse-velocity method with the capability of identifying charged-particles with $Z=1$, $Z=2$, and $Z>2$. The flow of neutrons was extracted from the slope at mid-rapidity of the curve of the average in-plane momentum vs the center-of-mass rapidity. The *squeeze-out* of the participant neutrons was observed in a direction normal to the reaction plane in the normalized momentum coordinates in the center-of-mass system. Experimental results of the neutron squeeze-out were compared with BUU calculations. The polar-angle dependence of the maximum azimuthal anisotropy ratio $r(\theta)$ was found to be insensitive to the mass of the colliding nuclei and the beam energy. Comparison of the observed polar-angle dependence of the maximum azimuthal anisotropy ratio $r(\theta)$ with BUU calculations for *free* neutrons revealed that $r(\theta)$ is insensitive also to the incompressibility modulus in the nuclear equation of state. [S0556-2813(99)03701-2]

PACS number(s): 25.75.Ld, 21.65.+f

I. INTRODUCTION

A primary goal of relativistic heavy-ion physics is to extract the equation-of-state (EOS) of nuclear matter. The EOS is the relationship between density, temperature, and pressure for nuclear matter [1–4]. Various experiments [5–15] have been undertaken in an effort to extract the EOS. In central collisions, the overlap regions of the target and the projectile form a compression zone of high density. Particles in this zone experience a deflection or outward flow from the interaction region. Measurements [9–11,15] with the plastic ball-wall detector [16] revealed three collective flow effects: the *bounce-off* of the spectators, the *side-splash* of the participants, and the *squeeze-out* of the participants in directions normal to the reaction plane. Measurements of the collective momentum flow in the collisions, including the flow angle [10,13] and the average transverse momentum in the reaction plane [6,7,9,15,17], were studied with a view toward extracting the nuclear EOS.

Zhang *et al.* [18] investigated the collective flow of neutrons correlated to the azimuthal distributions for semicentral Au-Au collisions at beam energies of 150, 250, 400, and 650 MeV per nucleon. Elaasar *et al.* [19,20] reported the first azimuthal distributions of triple-differential cross sections for neutrons emitted in Nb-Nb collisions at 400*A* MeV and examined the maximum azimuthal anisotropy ratios of these neutron cross sections as a probe of the nuclear equation of state by comparison with Boltzmann-Uehling-Uhlenbeck (BUU) calculations for *free* neutrons with a momentum-dependent interaction. Madey *et al.* [21] extended this comparison to 400*A* MeV Au-Au collisions and found that the maximum azimuthal anisotropy ratio does not depend on the mass of the colliding nuclei. Welke *et al.* [22] defined the maximum azimuthal anisotropy ratio $r(\theta)$ as a ratio of the maximum triple-differential cross section to the minimum triple-differential cross section at each polar angle.

In this paper, we report measurements of triple-differential cross sections of neutrons emitted in high-multiplicity La-La collisions at 250 and 400 *A* MeV (and Nb-Nb collisions at 400*A* MeV) as a function of the azimuthal angle with respect to the reaction plane for several polar angles. From these data and our prior data [18] for Au-Au collisions at 400*A* MeV, we examined the sensitivity of the *maximum azimuthal anisotropy ratio* $r(\theta)$ to the mass of three systems [viz., Nb-Nb, La-La, and Au-Au] and to the beam energy from 250 to 400 *A* MeV for the La-La system; we extracted the flow [9] of neutrons from the slope at midrapidity of the curve of the average in-plane momentum versus the neutron center-of-mass rapidity; and we observed the *out-of-plane squeeze-out* of neutrons in three systems [viz., 250 and 400 *A* MeV La-La, and 400*A* MeV Nb-Nb].

*Present address: CyberAccess Inc., Valley View, OH 44125.

†Present address: Southern University at New Orleans, New Orleans, LA 70126.

‡Present address: Picker International Inc., Cleveland, OH 44143.

§Present address: Crump Institute for Biological Imaging, UCLA School of Medicine, Los Angeles, CA 90095-1770.

‖Present address: University of Texas at Austin, Austin, TX 78712.

¶Present address: Texas A & M University, College Station, TX 77843.

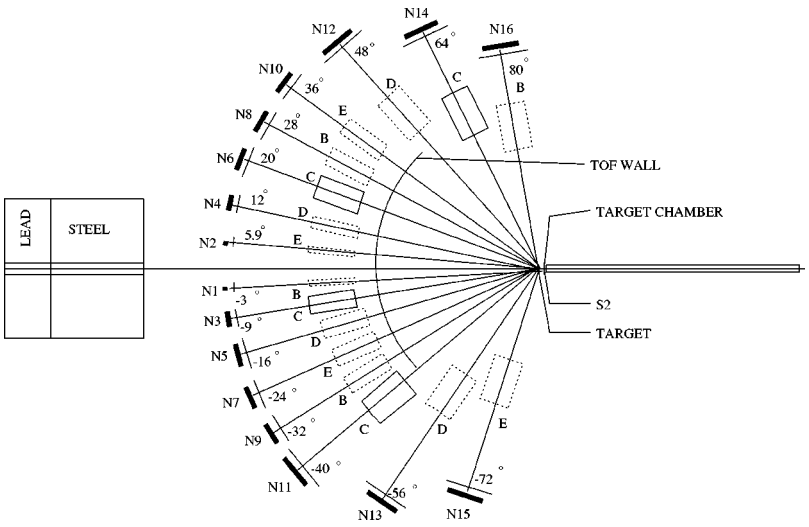

FIG. 1. Experimental arrangement.

II. EXPERIMENTAL APPARATUS

Based on experience gained from experiment 848H in 1988 [18,19], an extension of experiment 848H was performed with the Bevalac at the Lawrence Berkeley Laboratory (LBL) with the improved experimental arrangement shown in Fig. 1. This experiment was improved over the original version by adding the capability of identifying charged particles with $Z=1$, $Z=2$, and $Z>2$. With this improvement, data were obtained for La-La collisions at 250 and 400 A MeV and for Nb-Nb collisions at 400A MeV.

A beam telescope, consisting of two scintillators S_1 and S_2, was used to select and count valid projectile beam ions and to provide a fiducial timing signal for the measurement of the flight times to the time-of-flight (TOF) wall detectors and to the neutron detectors. Scintillator $S1$ was positioned 13.04 m upstream of the target in the beam. Scintillator $S2$ was placed immediately before the target. A total of 16 mean-timed neutron detectors [23–26] were placed at angles from 3° to 80° with flight paths ranging from 6 to 8.4 m. Table I shows the width, polar angle, and flight path of each neutron detector used in this experiment. The width of the neutron detector and the flight path at each angle were selected to provide approximately equal counting rates and energy resolutions for the highest energy neutrons at each angle. To avoid detecting charged particles in neutron detectors, 9.5-mm thick anticoincidence detectors were placed im-

TABLE I. Neutron detector placement and shadow shield configurations.

Detector No.	Width w (in)	Polar angle θ (deg)	Flight path x (m)	Distance from target to front of shield (m)	Configurations A	B	C	D	E
N16	20	80.0	6.00	3.0		*SS*4			
N14	20	64.0	7.00	3.5			*SS*4		
N12	20	48.0	8.00	4.5				*SS*4	
N10	10	36.0	8.40	4.8					*SS*3
N8	10	28.0	8.40	4.8		*SS*3			
N6	10	20.0	8.40	5.0			*SS*3		
N4	5	12.0	8.40	5.0				*SS*2	
N2	1	5.9	8.39	5.0					*SS*1
N1	1	−3.0	8.40	5.0		*SS*1			
N3	5	−9.0	8.40	5.0			*SS*2		
N5	10	−16.0	8.40	5.0				*SS*3	
N7	10	−24.0	8.40	5.0					*SS*3
N9	10	−32.0	8.40	4.8		*SS*3			
N11	20	−40.0	8.40	4.8			*SS*4		
N13	20	−56.0	7.50	3.8				*SS*4	
N15	20	−72.0	6.20	3.1					*SS*4
[3mm] Type	Dimensions (in^3)		Number						
*SS*1	5.5×40×40		1		0	1	0	0	1
*SS*2	8.0×36×43		1		0	0	1	1	0
*SS*3	14×40×42		2		0	2	1	1	2
*SS*4	20×40×42		2		0	1	2	2	1

mediately in front of the neutron detectors. The TOF of each detected neutron was determined by measuring the time difference between the detection of a neutron in one of the neutron detectors and the detection of a projectile ion in the beam telescope.

The azimuthal angle of the reaction plane was determined from the information given by a time-of-flight (TOF) wall, which consisted of 184 plastic scintillators, each with a thickness of 9.5 mm. The overall dimensions of the TOF wall were 5-m wide and 4.5-m high. The plastic wall was shaped as an arc around the target, and covered angles of $\pm 37°$ relative to the beam line. The flight paths of the TOF wall detectors varied from about 4.0 to 5.0 m.

To assess the background, steel shadow shields were positioned approximately half-way between the TOF wall and the neutron detectors in four different configurations (see Table I). The resulting spectra were then subtracted from the ones without shadow shields. We used a method introduced by Zhang *et al.* [18] to correct for an over-estimation of backgrounds by this shadow-shield subtraction technique.

III. DATA ANALYSIS

In order to suppress the background arising from collisions of beam ions and air molecules between the target and the TOF wall, an appropriate multiplicity-cut had to be made. Figure 2 shows the charged-particle multiplicity spectra with (solid line) and without (dashed line) the target for La-La and Nb-Nb collisions at 400*A* MeV and La-La collisions at 250*A* MeV. A proper multiplicity cut was chosen by comparing the charged-particle multiplicity spectra with and without the target in place. To make meaningful comparisons of the data for La-La and Nb-Nb collisions at 400*A* MeV and La-La collisions at 250*A* MeV, the multiplicity cuts chosen should correspond to approximately the same range in normalized impact parameter while keeping the background contaminations (from collisions of beam ions with the air or material in the beam telescope) below 5%. For La-La collisions at 400 and 250 *A* MeV, the appropriate charged-particle multiplicity cuts were found to be 34 and 30, respectively, whereas a multiplicity cut of 25 was determined for Nb-Nb collisions at 400*A* MeV. From the relationship between the total number of interactions expected from the geometric cross section of the system and with the well-known assumption [19,27] of a monotonic correlation between the impact parameter and the fragment multiplicity, the maximum impact parameter normalized to the radii of the projectile and target $b_{\max}/(R_p+R_t)$ was found to be about 0.5 for the above multiplicity cuts. The method of extracting the maximum-normalized impact parameter $b_{\max}/(R_p+R_t)$ can be found in Ref. [20].

A. Determination of reaction plane

To study flow, it is necessary to determine the reaction plane (i.e., the xz plane), where $\hat{x}$ is in the direction of the impact parameter of the collision and $\hat{z}$ is in beam direction. The reaction plane was determined by a modified version [28] of the transverse momentum method [7]. The charged particles emitted from the collisions between beam ions and the target were detected by the TOF wall detectors. The azimuthal angle Φ_R of the reaction plane was estimated from the vector $\vec{Q}^{\nu}$, the weighted sum of the transverse velocity vectors $\vec{V}^t$ of all charged fragments detected in each collision:

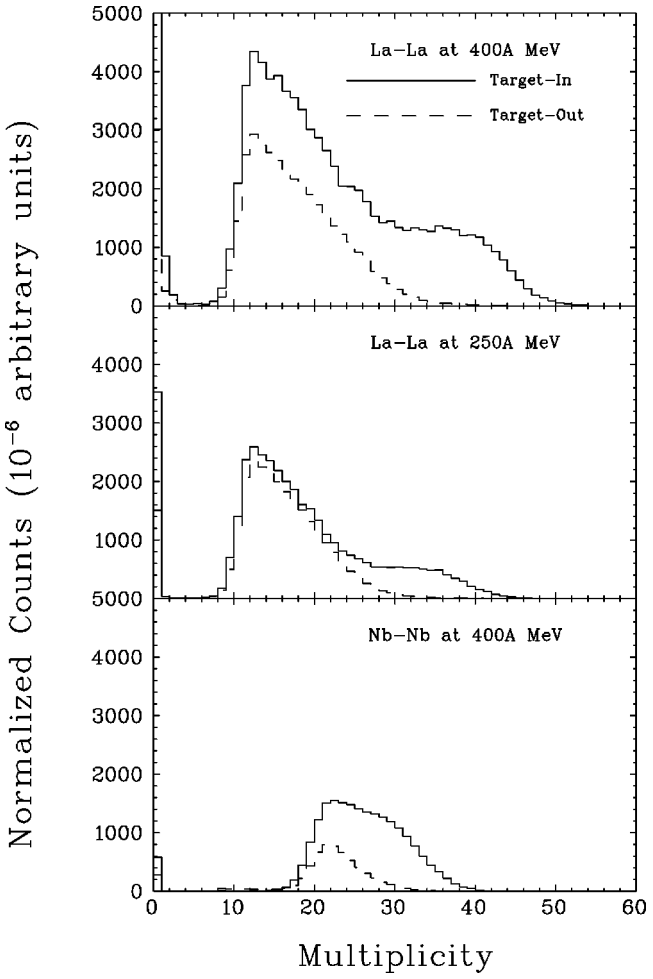

FIG. 2. Charged-particle multiplicities with and without the target in place for La-La collisions at 400 and 250 *A* MeV, and Nb-Nb collisions at 400*A* MeV.

$$\vec{Q}^{\nu}=\sum_i \nu_i\left(\frac{\vec{V}^t}{|\vec{V}^t|}\right)_i, \tag{1}$$

where the weight ν_i depends on the pulse height of the ith charged particle. The values of the ν_i are positive for $\alpha \geqslant \alpha_0$ and zero for $\alpha<\alpha_0$, where the quantity $\alpha \equiv (Y/Y_p)_{\text{c.m.}}$ is the rapidity Y normalized to the projectile rapidity Y_p in the center-of-mass system, and α_0 is a threshold rapidity. The rapidity Y of a charged particle with an identified Z was calculated with an assumption that its mass is the mass of proton, ^{4}He, and ^{7}Li, respectively, for $Z=1$, 2, and $Z>2$. The dispersion angle $\Delta\phi_R$, the angle between the *estimated* and *true* reaction planes, is defined [29] as

$$\cos\Delta\phi_R=\frac{\langle V_x'\rangle}{\langle V_x\rangle}, \tag{2}$$

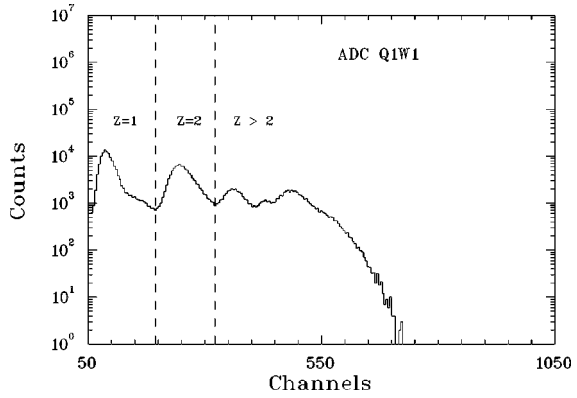

FIG. 3. Pulse-height spectrum from 400*A* MeV La-La collisions for one of the 184 detectors in the time-of-flight wall.

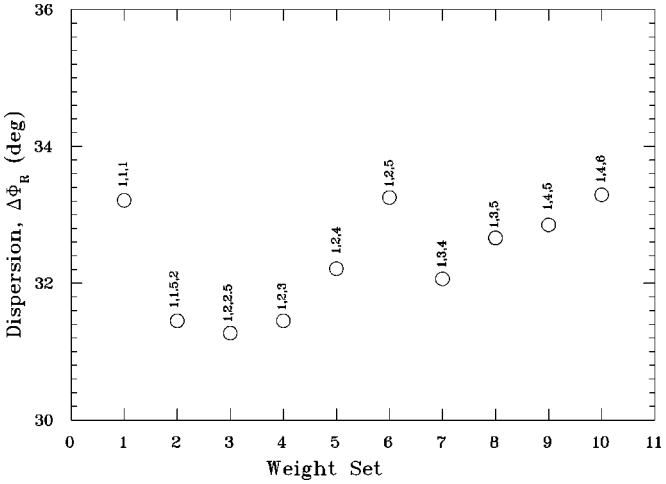

FIG. 4. Dispersion $\Delta\phi_R$ in the azimuthal reaction plane angle ϕ_R with different sets of weights tuned for $Z=1$, $Z=2$, and $Z>2$ isotopes for La-La collisions at 400*A* MeV. Each set of weights consists of three numbers assigned, respectively, to the charged particles with $Z=1$, $Z=2$, and $Z>2$. Among ten sets of weights used to calculate dispersion angle $\Delta\Phi_R$, the set (1, 2, 2.5) gives a minimum dispersion angle.

where $\langle V_x' \rangle$ and $\langle V_x \rangle$ are projections of unit vectors onto the *estimated* and the *true* reaction plane, respectively. All the results presented in this report are corrected for this dispersion.

The smaller the dispersion angle, the closer the *estimated* reaction plane to the *true* one. By averaging the projection of the unit vector $(\vec{V}^t/|\vec{V}^t|)_i$ onto the *true* reaction plane over the total events, one can obtain

$$\langle V_x \rangle = \left[\frac{\overline{Q^2 - W}}{\overline{W(W-1)}} \right]^{1/2}; \quad \vec{Q} = \sum_i \omega_i \left(\frac{\vec{V}^t}{|\vec{V}^t|} \right)_i ,$$

$$W = \sum_i \omega_i , \tag{3}$$

where i is the particle index. The weight ω_i in the above equation is equal to unity for $\alpha \geqslant \alpha_0$ and is equal to zero for $\alpha < \alpha_0$.

The average of the normalized in-plane vector of all charged particles projected onto the *estimated* reaction plane $\langle V_x' \rangle$ can be estimated by

$$\langle V_x' \rangle = \overline{\left(\frac{\vec{V}^t}{|\vec{V}^t|} \right)_i \frac{\vec{Q}_i^{\nu}}{|\vec{Q}_i^{\nu}|}}; \quad \vec{Q}_i^{\nu} = \sum_{j \neq i} \nu_j \left(\frac{\vec{V}^t}{|\vec{V}^t|} \right)_j \tag{4}$$

where the weight ν_j depends on the pulse height of the charged particles. The weighting factors ν_j were chosen to minimize the dispersion angle $\Delta\phi_R$. For different values of ν_j, the dispersion angles for La-La collisions at 250 and 400 *A* MeV and Nb-Nb collisions at 400*A* MeV exhibit a broad minimum (around $\alpha_0 = 0.2$) as a function of the threshold rapidity α_0; to minimize the dispersion, we chose $\alpha_0 = 0.2$.

Figure 3 shows a typical pulse-height spectrum for one of the 184 TOF wall detectors for La-La collisions at 400*A* MeV. The peak labeled $Z=1$ is from hydrogen isotopes; that labeled $Z=2$ is from helium isotopes. The third and the following peaks labeled $Z>2$ represent charged particles with $Z>2$. Based on these peaks, three different sets of weights were tuned to estimate the reaction plane closest to the true reaction plane. Figure 4 shows the dispersion angles obtained at different sets of weights for La-La collisions at 400*A* MeV. The uncertainties in this figure were not calculated because our main interest was to minimize the values of the dispersion angles. In this work, ten sets of weights (as shown in Fig. 4) were used to calculate the dispersion angles. The weights 1, 2, and 2.5 for $Z=1$, $Z=2$, and $Z>2$ isotopes, respectively, yielded a minimum value for the dispersion $\Delta\phi_R$ in ϕ_R. With these weights, the dispersion angles from Eq. (2) were found to be $31.3° \pm 2.4°$ and $33.8° \pm 2.3°$ for La-La collisions at 400 and 250 *A* MeV, respectively, and $39.8° \pm 3.0°$ for Nb-Nb collisions at 400*A* MeV. Without the charged-particle identification (i.e., $\nu_j = 1$), Eq. (4) corresponds to that in Ref. [18,19]; the dispersion angles were about 3° larger in these three sets of data. After the azimuthal angle ϕ_R of the reaction plane was determined, the neutron azimuthal angle relative to the reaction plane ($\phi - \phi_R$) was obtained for each event.

B. Determination of the flow axis

To study the emission patterns and the event shapes of the fragments, the sphericity method [30] was used. From a set of charged particles in the center-of-mass system for each event, a sphericity tensor is defined as

$$F_{ij} = \sum_{\nu} \frac{1}{2m_{\nu}} \frac{V_i^{\nu} V_j^{\nu}}{|V^{\nu}|^2}, \tag{5}$$

where m_{ν} is the mass of the νth fragment, which can be one of the protonlike ($Z=1$), heliumlike ($Z=2$), or ''lithium-like'' ($Z>2$) particles identified by pulse-heights in the TOF wall as mentioned in the previous section. In the sphericity calculation, we omitted all tracks in the backward rapidity range ($\alpha<0$), then we projected the tracks in the forward rapidity range ($\alpha>0$) to the backward rapidity range $\vec{V} \rightarrow -\vec{V}$. Our sphericity calculations reconstructed polar flow angles, which allowed neutron squeeze-out to become vis-

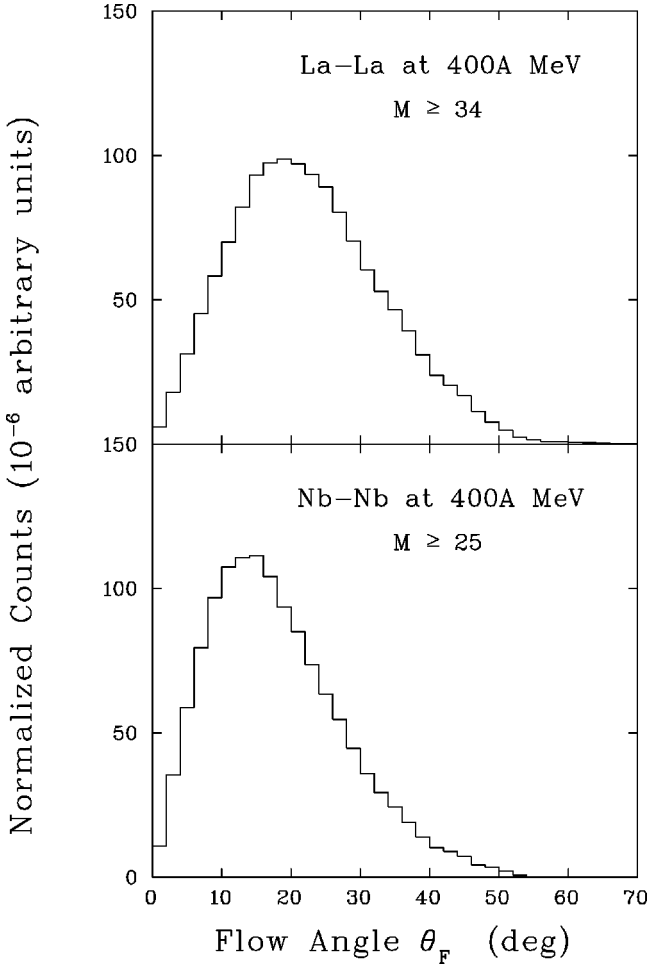

FIG. 5. Distribution of the flow angle (θ_F) for La-La and Nb-Nb collisions at 400*A* MeV with the same impact parameter (in the units of the nuclear radius) ($b/2R$) = 0.51.

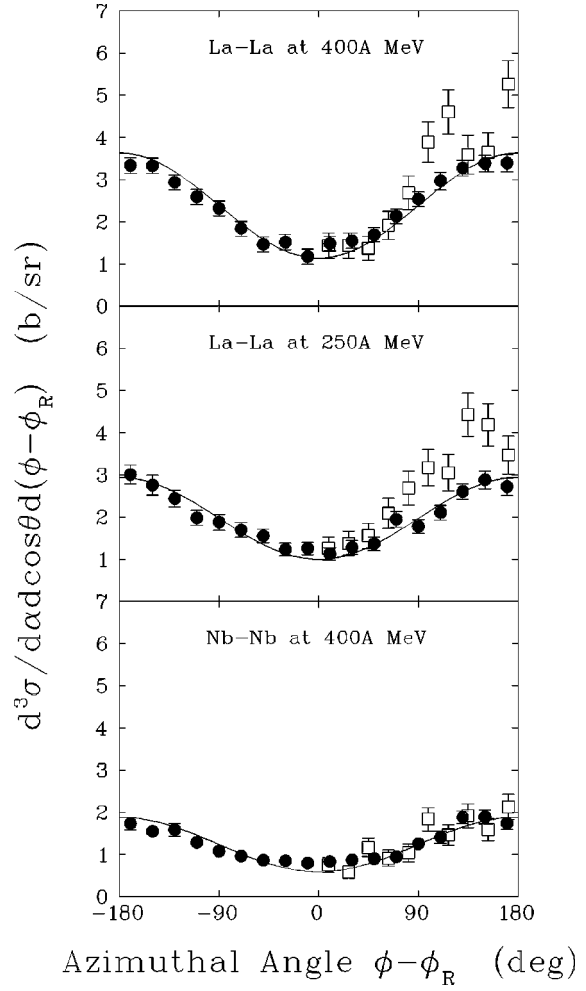

FIG. 6. Triple-differential cross sections for the emissions of neutrons in the backward rapidity bin ($-1.0 \leqslant \alpha < -0.2$) at a polar angle of $\theta = 72°$ from La-La collisions at 400 and 250 *A* MeV, and Nb-Nb collisions at 400*A* MeV. The open symbols represent BUU theory with $K = 215$ MeV for *free* neutrons with a critical distance $d_c = 2.8$ fm. The filled symbols represent the data, and the solid line represents the data corrected to zero dispersion $\Delta\phi_R = 0$.

ible. By diagonalizing the flow tensor in the center-of-mass system, the event shape can be approximated as a prolate (or cigar-shaped) ellipsoid. The angle between the major axis of the flow ellipsoid and the beam axis is defined as a flow angle θ_F.

Quantitatively, the flow angle [10] was obtained as a polar angle corresponding to the maximum eigenvalues of the flow tensor. Figure 5 shows the distribution of the flow angle θ_F for La-La and Nb-Nb collisions at 400*A* MeV with the same impact parameter. For Nb-Nb and La-La collisions at the same energy, the peak of the neutron flow angle distribution moves to a larger angle as the mass of the system increases. This trend to larger flow angles with increasing target-projectile mass was observed previously for charged particles [13] by the plastic ball spectrometer, and predicted qualitatively from Vlasov-Uehling-Uhlenbeck calculations [31].

IV. RESULTS

A. Neutron triple-differential cross sections

The results of the triple-differential cross sections $d^3\sigma/d\alpha d\cos\theta d(\phi-\phi_R)$, for neutrons emitted at a polar angle θ with a normalized center-of-mass rapidity $\alpha \equiv (Y/Y_p)_{\text{c.m.}}$ (in units of the projectile rapidity Y_p) are presented as a function of the azimuthal angle ($\phi-\phi_R$) with respect to the reaction plane. The data were summed in four rapidity bins ($\Delta\alpha$) for each detector: backward rapidities ($-1.0 \leqslant \alpha < -0.2$), midrapidities ($-0.2 \leqslant \alpha < 0.2$), intermediate-forward rapidities ($0.2 \leqslant \alpha < 0.7$), and projectilelike rapidities ($0.7 \leqslant \alpha < 1.2$). The uncertainties in the triple-differential cross sections include both statistical and systematic uncertainties; however, statistical uncertainties dominate systematic uncertainties [20].

Figure 6 shows the triple-differential cross sections for neutrons emitted in the backward rapidity bin at a polar angle of 72° for La-La and Nb-Nb collisions at 400*A* MeV and La-La collisions at 250*A* MeV. The cross sections in this rapidity bin have a minimum at ($\phi-\phi_R$) = 0° and a maximum at ($\phi-\phi_R$) = ±180°. Similar characteristics can be found at other polar angles, ranging from 3° to 80°.

Figure 7 shows the neutron triple-differential cross sections for the midrapidity bin at one of the polar angles (viz., $\theta = 48°$) for La-La and Nb-Nb collisions at 400*A* MeV and La-La collisions at 250*A* MeV. In this bin, the neutrons are

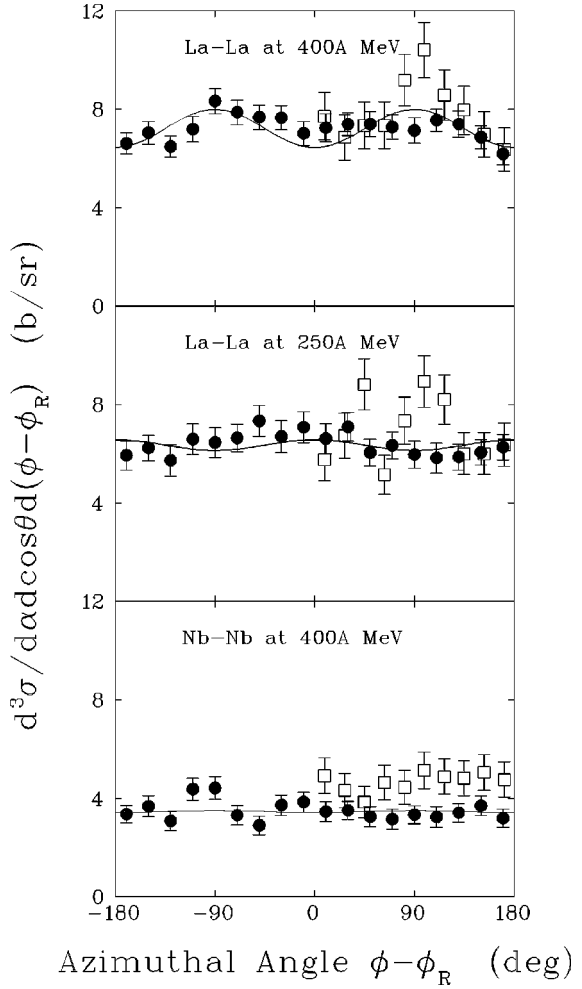

FIG. 7. Triple-differential cross sections for the emission of neutrons in the midrapidity bin ($-0.2 \leqslant \alpha < 0.2$) at a polar angle of 48° from La-La collisions at 400 and 250 A MeV, and Nb-Nb collisions at 400A MeV. The open symbols represent BUU theory with $K=215$ MeV for *free* neutrons with a critical distance $d_c=2.8$ fm. The filled symbols represent the data and the solid line represents the data corrected to zero dispersion $\Delta\phi_R=0$.

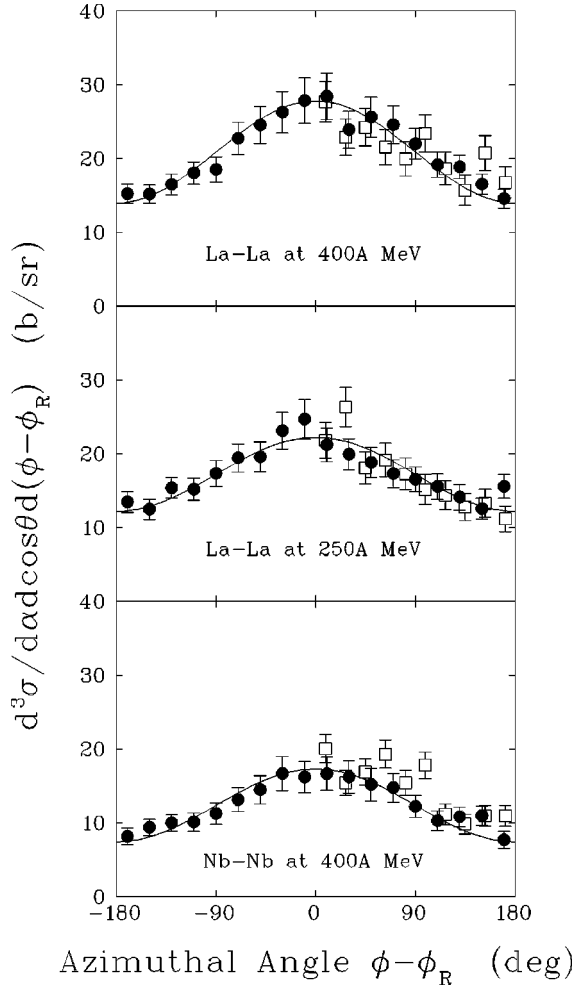

FIG. 8. Triple-differential cross sections for the emission of neutrons in the projectile rapidity bin ($0.7 \leqslant \alpha < 1.2$) at a polar angle of 16° from La-La collisions at 400 and 250 A MeV, and Nb-Nb collisions at 400A MeV. The open symbols represent BUU theory with $K=215$ MeV for *free* neutrons with a critical distance $d_c=2.8$ fm. The filled symbols represent the data and the solid line represents the data corrected to zero dispersion $\Delta\phi_R=0$.

aligned perpendicular to the reaction plane at $(\phi-\phi_R)=\pm 90°$ (so called squeeze-out) [11,12,14]; however, this effect is barely noticeable in our figures. Rotating the event onto the flow axis enhances our ability to see the squeeze-out effect [11,32].

Figure 8 shows the neutron triple-differential cross sections for the projectile rapidity bin at a polar angle 16° (as an example) for La-La and Nb-Nb collisions at 400A MeV and La-La collisions at 250A MeV. At each polar angle, the azimuthal distribution for this rapidity bin peaks at $(\phi-\phi_R)=0°$ and has a minimum at $(\phi-\phi_R)=\pm 180°$. The peak at 0° is the result of the side-splash and bounce-off effects, where bounce-off cannot be separated clearly from the side-splash. The resulting cross sections in these projectile rapidities also have contributions from both participants and spectators such as those at target or backward rapidities; however, the side-splash dominates at the larger polar angles where the collisions are more central because of the multiplicity cut chosen for this analysis.

Finally, Fig. 9 shows the neutron triple-differential cross sections for the intermediate-forward rapidity bin at the polar angle 20° for La-La and Nb-Nb collisions at 400A MeV and La-La collisions at 250A MeV. The distributions at small polar angles in this rapidity bin reflect the distributions in the midrapidity bin. The larger the polar angles, the more noticeable the peaks at $(\phi-\phi_R)=0°$ and the distributions become more similar to the distributions from the projectile rapidity regions.

B. Average in-plane momentum

Figure 10 shows the mean transverse momentum projected into the reaction plane $\langle P_x \rangle$ for neutrons as a function of normalized center-of-mass rapidity $\alpha=(Y/Y_p)_{\text{c.m.}}$, for La-La collisions at an energy of 400 and 250 A MeV. The technique of extracting the $\langle P_x \rangle$ for neutrons can be found in Ref. [18].

The data display the typical S-shaped behavior as described by Danielewicz and Odyniec [7]. Neutrons in the low-energy regions (below $\approx$ 55 MeV) were not included in order to eliminate background contamination; thus, the curve is not completely symmetric and the slope of the average

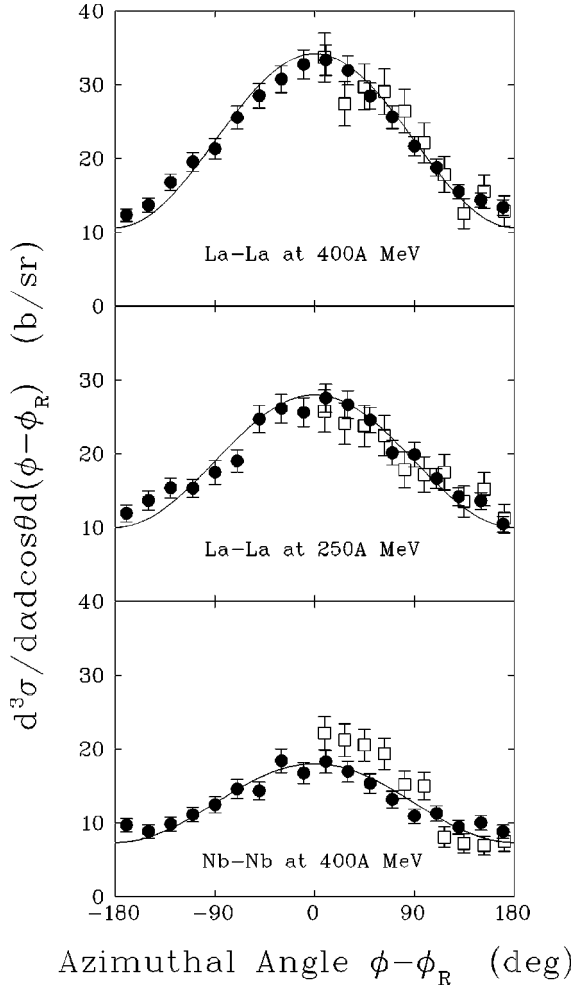

FIG. 9. Triple-differential cross sections for the emission of neutrons in the intermediate-forward rapidity bin ($0.2 \leqslant \alpha < 0.7$) at a polar angle of 20° from La-La collisions at 400 and 250 *A* MeV, and Nb-Nb collisions at 400*A* MeV. The open symbols represent BUU theory with $K=215$ MeV for *free* neutrons with a critical distance $d_c=2.8$ fm. The filled symbols represent the data and the solid line represents the data corrected to zero dispersion $\Delta\phi_R=0$.

in-plane transverse momentum at negative rapidities is steeper than that at positive rapidities because the cut on the low-energy neutrons rejects neutrons with low transverse momenta at negative rapidities. From Fig. 10, the average in-plane momentum increases with increasing bombarding energies.

In the positive rapidity region, the $\langle P_x \rangle$ vs α curves are straight lines up to $\alpha=0.5$. We extracted the slope at midrapidity (up to $\alpha=0.5$) with a linear fit to $\langle P_x \rangle$ in the region unaffected by the cut on the neutron energy; Doss *et al.* [9] defined this slope as the *flow F*. Because the flow is determined at midrapidity, it has contributions only from the participants. The flows found in this analysis are 145 ± 11 and 104 ± 13 MeV/*c* from La-La collisions at 400 and 250 *A* MeV, respectively. From these data, we see that the neutron flow increases with increasing beam energy. Previously, Doss *et al.* [9] observed that the flow of charged particles increases with beam energy, reaches a broad maximum at about 650*A* MeV, and falls off slightly at higher energies.

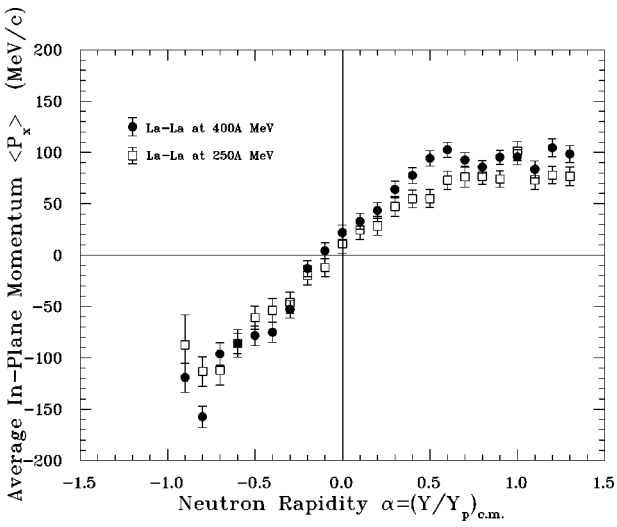

FIG. 10. Average in-plane momentum projected into the reaction plane for neutrons from La-La at 400 and 250 *A* MeV as a function of the normalized rapidity of the neutrons in the center-of-mass system.

C. Neutron squeeze-out

One of the results of this experiment is the observation of neutrons emitted preferentially in a direction perpendicular to the reaction plane. In their paper reporting this component of collective flow for charge particles, Gutbrod *et al.* [11] called this collective phenomenon *out-of-plane squeeze-out.*

To see neutron squeeze-out, we performed two coordinate rotations: First, we rotated the *x* coordinate around the beam or *z* axis to align it with the summed transverse-velocity vector $\vec{Q}$ given by Eq. (3); second, we rotated the *z* axis around the *y* axis by the flow angle Θ_F. After this second rotation, the z' axis of the new $x'y'z'$ coordinates, where $y'=y$, is on the major axis of flow ellipsoid. Then, for neutrons with transverse momenta p_z' in the region $-0.1 \leqslant p_z' < 0.1$, where $p_z'=(P_z'/P'_{\rm proj})_{\rm c.m.}$, neutron squeeze-out became visible as a peak at azimuthal angles $\phi'=\pm90°$ for the distribution in the $x'y'$ plane. Figure 11 shows the neutron azimuthal distributions in the $x'y'$ coordinates or neutron squeeze-out of three systems: La-La and Nb-Nb collisions at 400*A* MeV and La-La collisions at 250*A* MeV. The spectator neutrons are excluded from Fig. 11 by removing neutrons of high and low momenta at small angles. By excluding spectator neutrons [8] emitted from the projectile and the target, neutrons evaporated [33,34] from an excited projectile at small polar angles ($\theta \leqslant 8°$) were excluded also. Squeeze out of neutrons was observed previously [14] for Au-Au collisions at 400*A* MeV.

V. THEORETICAL COMPARISONS

Welke *et al.* [22] examined the sensitivity of $d\sigma/d\phi$ to the nuclear matter equation of state. Because there was a net flow in the projectile and target rapidity bins, Welke *et al.* described the shapes of the azimuthal distribution by the ratio of the maximum cross section $(d\sigma/d\phi)_{\rm max}$ to the minimum cross section $(d\sigma/d\phi)_{\rm min}$.

For each polar angle, the cross sections measured in the experiment are fitted with the function $\sigma_3(\phi-\phi_R,\theta)$

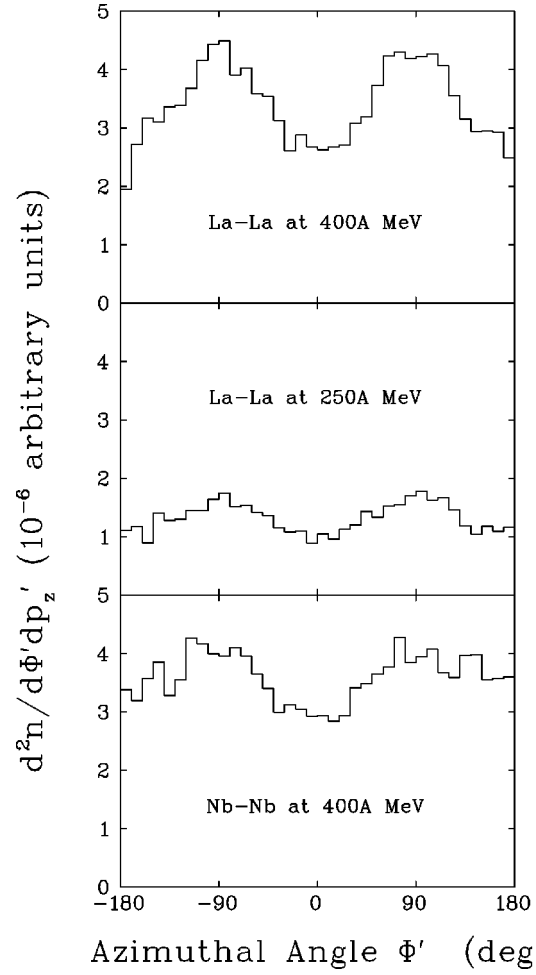

FIG. 11. Azimuthal distribution (ϕ') of the neutrons around the flow axis or neutron squeeze-out in the momentum region $[-0.1 \leq p_z' = (P_z'/P_{\text{proj}}')_{\text{c.m.}} \leq 0.1]$ for La-La collisions at 400 and 250 A MeV, and Nb-Nb collisions at 400A MeV.

$= a(\theta) \pm b'(\theta)\cos(\phi - \phi_R)$, where the $+(-)$ sign stands for positive (negative) rapidity bin, and $b'(\theta) = b(\theta)e^{-(\Delta\phi_R)^2/2}$ is the correction for a finite rms dispersion $\Delta\phi_R$. For positive rapidity particles, the cross sections peak at $(\phi - \phi_R) = 0°$ and deplete at $(\phi - \phi_R) = \pm 180°$, as seen in Fig. 8. The maximum azimuthal anisotropy for positive rapidity neutrons becomes $r(\theta) = [a(\theta) + b(\theta)]/[a(\theta) - b(\theta)]$. Figure 12 is the polar-angle-dependent maximum azimuthal anisotropy ratio $r(\theta)$ for the four sets of data as indicated; the data for Au-Au collisions at 400A MeV are from Elaasar *et al.* [20]. From Fig. 12, the maximum azimuthal anisotropy appears to be independent of both the mass of the colliding nuclei and the beam energy.

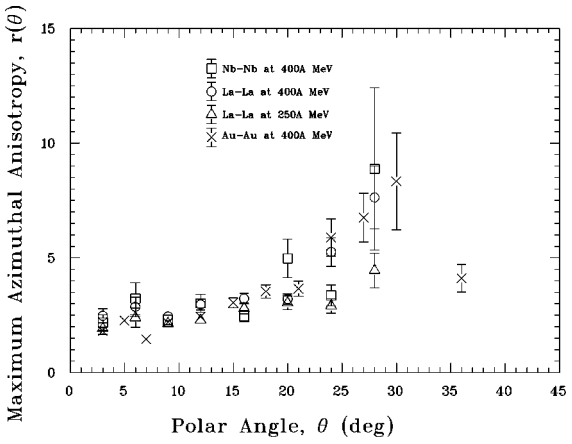

FIG. 12. The polar-angle-dependent maximum azimuthal anisotropy ratio $r(\theta)$ as a function of the polar angle θ for La-La and Nb-Nb collisions at 400A MeV and La-La collisions at 250A MeV in the projectile rapidity bin $(0.7 \leq \alpha < 1.2)$. The data for Au-Au collisions at 400A MeV is reproduced from Elaasar *et al.* [20]

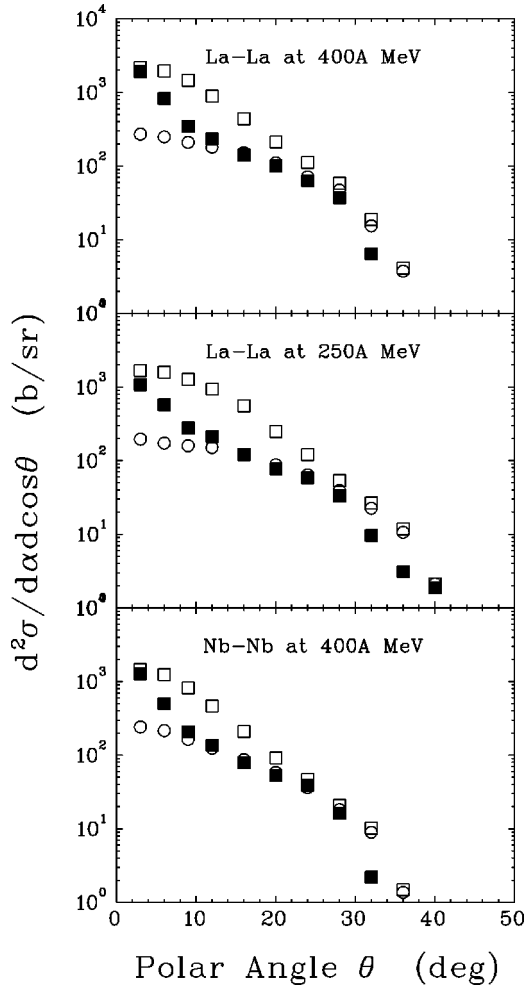

FIG. 13. Polar-angle dependence of the double-differential cross sections for neutrons emitted with rapidities $0.7 \leq \alpha < 1.2$ from La-La collisions at 400 and 250 A MeV, and Nb-Nb collisions at 400A MeV. The filled squares represent the data and the open symbols represent BUU theory with $K = 215$ MeV: open squares represent *all* neutrons and open circles represent neutrons that are not in clusters or *free* neutrons.

For theoretical comparison, we used the Boltzmann-Uehling-Uhlenbeck (BUU) approach [35] with a parametrization of a momentum-dependent nuclear mean field suggested in Ref. [22]. In the calculations, the incompressibility modulus K was set to be 215 MeV, and the contributions to the cross sections from composite fragments were subtracted by rejecting neutrons when the distance between the neutron and another nucleon from the same BUU ensemble [35] was less than a critical value d_c [36]. Within a given BUU run, a nucleon was considered *free* only if no other nucleons were found within the critical distance d_c. We are justified in restricting our coalescence criterion to coordinate space as

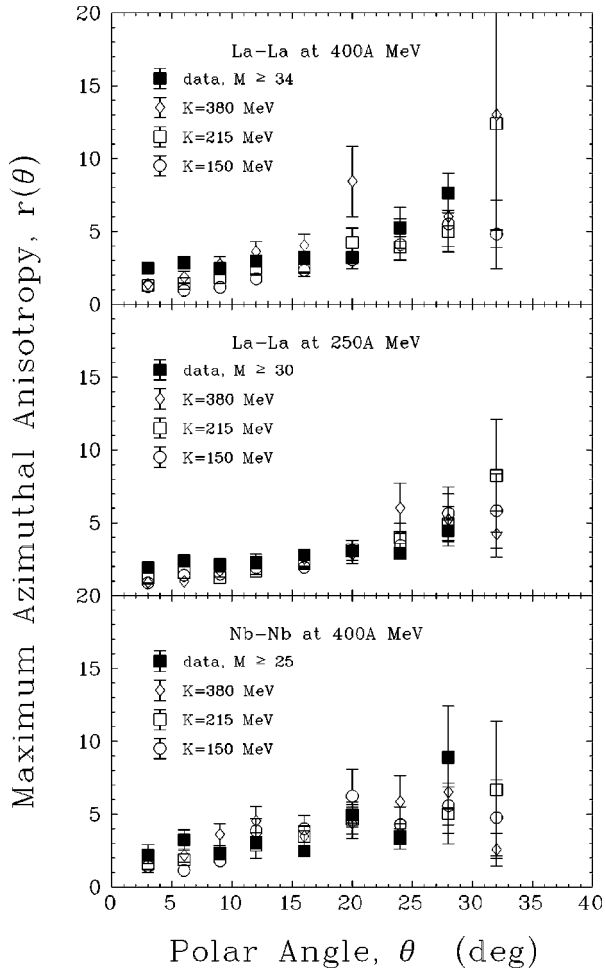

FIG. 14. The polar-angle-dependent maximum azimuthal anisotropy ratio $r(\theta)$ as a function of the polar angle θ for La-La and Nb-Nb collisions at 400*A* MeV and La-La collisions at 250*A* MeV from BUU calculations with $K=380$, 215, 150 MeV. The value $d_c=2.8$ fm was used for these systems. The results for Au-Au collisions at 400*A* MeV with $d_c=3.2$ fm is reproduced from Elaasar *et al.* [19]

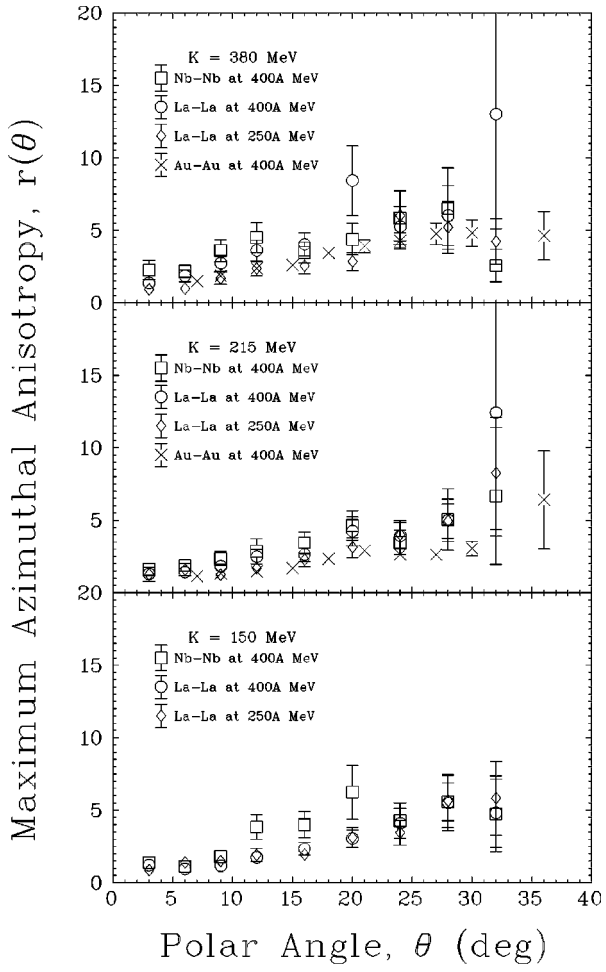

FIG. 15. The polar-angle-dependent maximum azimuthal anisotropy ratio $r(\theta)$ as a function of the polar angle θ for La-La collisions at 400 and 250 *A* MeV, and Nb-Nb collisions at 400*A* MeV. The filled squares represent the data and the open symbols represent BUU theory with $K=380$ MeV, $K=215$ MeV, and $K=150$ MeV as indicated in the figure.

nucleons that are far apart in momentum space will have drifted away from each other. Our analysis is performed at the time that the momentum space distributions begin to freeze-out [37]. Also we have verified quantitatively the soundness of this argument by performing a full six-dimensional coalescence. It is well known from transport theory calculations that the transverse momentum generation in heavy-ion reactions begins quite early in the history of the reaction and then saturates [38]. For *free* neutrons, the critical distance d_c was chosen to be 2.8 fm for both Nb-Nb and La-La at 400*A* MeV and 3.0 fm for La-La at 250*A* MeV by fitting the polar-angle dependence of the double-differential cross sections. The double-differential cross sections in the rapidity $0.7\leqslant\alpha<1.2$ bin for La-La and Nb-Nb collisions at beam energy 400*A* MeV and La-La collisions at 250*A* MeV are shown in Fig. 13. The filled symbols represent the data, and the open symbols represent the BUU calculations. The BUU calculations (with $d_c=0$ fm) of the double differential cross sections are significantly higher than the data because the data do not include the composite fragments; in other words, the data contain *free* neutrons only. For $d_c=2.8$ fm, the BUU prediction is lower than the data at small polar angles because the BUU calculations do not treat neutron evaporation which occurs at polar angles below $\sim 9°$, as observed previously by Madey *et al.* [34].

By restricting the BUU calculations to *free* neutrons with $K=215$ MeV, the triple-differential cross sections are compared with data. Figures 6–9 show triple-differential cross sections for four rapidity regions: $-1.0\leqslant\alpha<-0.2$, $-0.2\leqslant\alpha<0.2$, $0.7\leqslant\alpha<1.2$, $0.2\leqslant\alpha<0.7$. In these figures, the open symbols represent the BUU calculations. The solid line in each figure represents the data corrected to zero dispersion $\Delta\phi_R=0$. In these calculations, the negative $(\phi-\phi_R)$ region is symmetric with respect to the positive side. In Fig. 6, the BUU results are higher than the data beyond $(\phi-\phi_R)=90°$. In Fig. 7, the BUU results tend to peak at $(\phi-\phi_R)=90°$; in other words, the BUU results show the characteristics of the out-of-plane squeeze-out effect for *free* neutrons in the midrapidity bin, but it is very hard to see the squeeze-out phenomena in the rapidity coordinates (see Sec. IV C). In Figs. 8 and 9, the BUU results generally agree with the data in these positive rapidity bins.

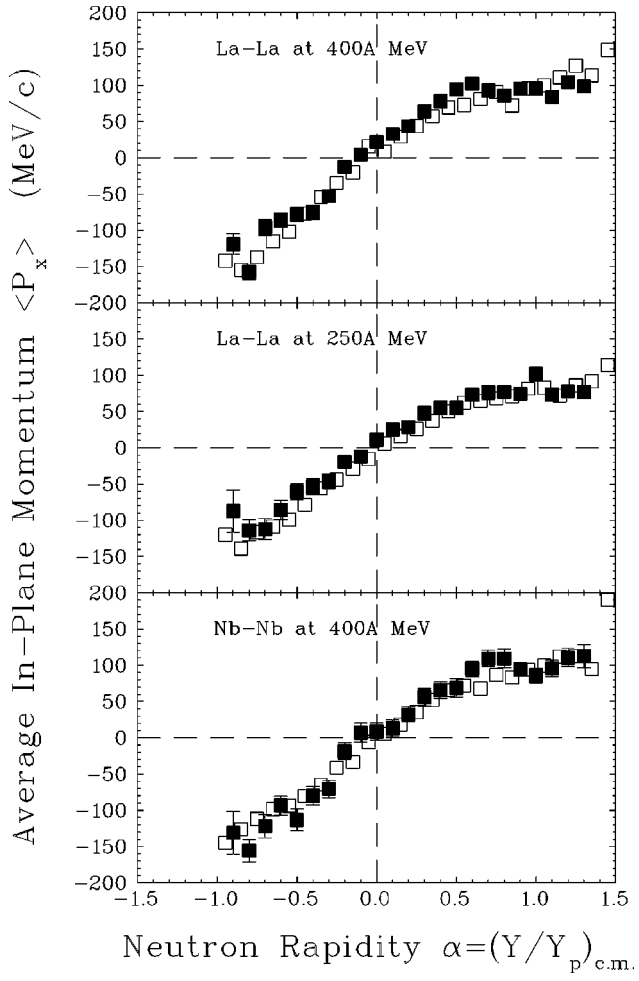

FIG. 16. Average in-plane momentum projected into the reaction plane for neutrons from La-La collisions at 400 and 250 A MeV, and Nb-Nb collisions at 400A MeV as a function of the normalized rapidity of the neutrons in the center-of-mass system. The filled squares represent the data and the open symbols represent BUU theory with $K=215$ MeV for *free* neutrons with a critical distance $d_c=2.8$ fm.

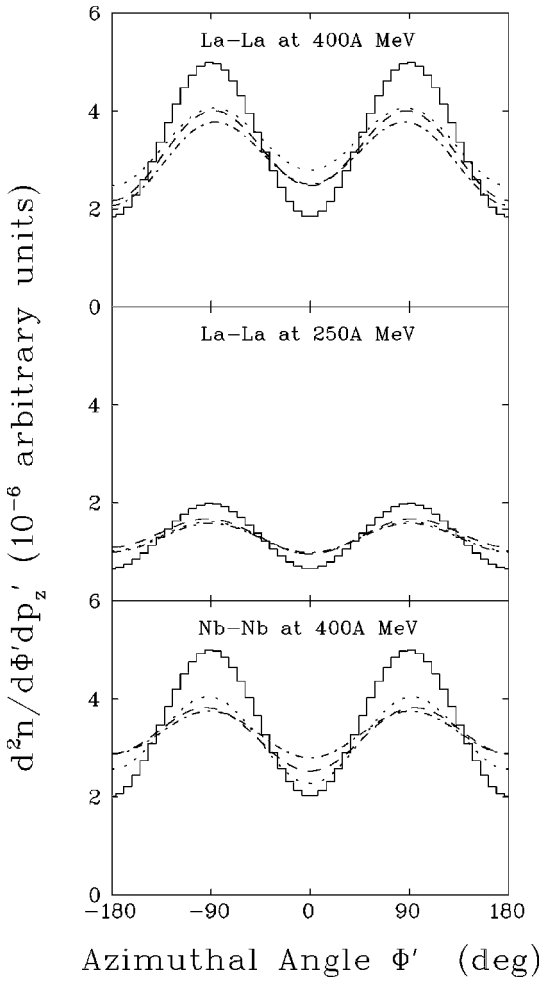

FIG. 17. Neutron squeeze-out in the mid-momentum $[-0.1 \leqslant p_z'=(P_z'/P'_{\rm proj})_{\rm c.m.} \leqslant 0.1]$ region for La-La collisions at 400 and 250A MeV, and Nb-Nb collisions at 400A MeV. The solid lines represent the data. The dotted, dashed, and dot-dashed lines represent BUU theory with $K=380$, 215, and 150 MeV, respectively, for *free* neutrons with a critical distance $d_c=2.8$ fm. All three lines are almost on top of each other in La-La collisions at 250A MeV.

The BUU calculations of the polar-angle dependence of the maximum azimuthal anisotropy ratio $r(\theta)$ for *free* neutrons emitted from Nb-Nb, La-La, and Au-Au collisions at 400A MeV and La-La collisions at 250A MeV are shown in Fig. 14 for $(b_{\rm max}/2R)=0.5$. The BUU results for Au-Au collisions at 400A MeV are from Elaasar *et al.* [20]. In this figure, the BUU calculations with $K=380$, 215, 150 MeV were carried out for *free* neutrons (with $d_c=2.8$ fm for Nb-Nb and La-La collisions and $d_c=3.2$ fm for Au-Au collisions). Consistent with the experimental data (see Fig. 12), the BUU calculations in Fig. 14 show little sensitivity to the mass and the beam energy. The BUU calculations of the polar-angle-dependent maximum azimuthal anisotropy ratio $r(\theta)$ for *free* neutrons emitted from La-La and Nb-Nb collisions at 400A MeV and La-La collisions at 250A MeV are compared with the data in Fig. 15. The multiplicity cuts indicated in this figure correspond to the ratio of the maximum impact parameter to the nuclear radius $(b_{\rm max}/2R)=0.5$. The filled and open symbols in this figure represent the data and the BUU calculations (with $K=150$, 215, 380 MeV), respectively. Both the experimental results and the BUU calculations were for zero dispersion $\Delta\phi_R=0$. As one can see from this figure, the polar-angle dependence of the maximum azimuthal anisotropy ratio $r(\theta)$ is insensitive to the incompressibility modulus K in the nuclear equation of state. This insensitivity was noted also in Ref. [37].

Figure 16 is the comparison between data and the BUU calculations with $K=215$ MeV for in-plane transverse momentum $\langle P_x\rangle$ for *free* neutrons emitted from La-La and Nb-Nb collisions at 400A MeV and La-La collisions at 250A MeV. Similar to the other figures, the filled symbols and open symbols represent the data and the BUU calculations, respectively. The BUU calculations generally agree with the data within their uncertainties, especially in the midrapidity region which gives the information about flow in the unit of MeV/c (see Sec. IV B).

Another observable obtained from BUU calculations is the out-of-plane squeeze-out of *free* neutrons. The comparisons are depicted in Fig. 17 for La-La and Nb-Nb collisions at 400A MeV and La-La collisions at 250A MeV. The solid

lines represent the data. The dotted, dashed, and dot-dashed lines represent the BUU calculations with $K=380$, 215, and 150 MeV, respectively. All three lines are almost on top of each other in La-La collisions at 250*A* MeV. The squeeze-out of neutrons in the normalized momentum coordinates in the center-of-mass system is compared with the BUU model. Both the experimental results and the BUU calculations are for zero dispersion $\Delta\phi_R=0°$. After correcting to zero dispersion in the experimental results, the neutron squeeze-out becomes larger. It can be seen from Fig. 17 that the squeeze-out of *free* neutrons from BUU calculations is insensitive to the incompressibility modulus K. From the comparison between the BUU calculations and the neutron squeeze-out in Fig. 17, the squeeze-out effect from the experimental data in this work is significantly stronger than that from the BUU calculations with $K=380$, 215, 150 MeV. It remains to be seen whether the apparent disagreement between the BUU squeeze-out results and the data persist as greater statistics and accuracy are reached for the calculations. We estimate the present uncertainties to be of the order of 25%. Statistically meaningful calculations of squeeze-out in BUU remain challenging as the effect truly needs to be established at a level past fluctuations.

VI. CONCLUSIONS

We measured triple-differential cross sections of neutrons emitted at several polar angles in multiplicity-selected La-La collisions at 250 and 400 A MeV (and Nb-Nb collisions at 400*A* MeV) as a function of the azimuthal angle with respect to the reaction plane. We compared the measured cross sections with BUU calculations for free neutrons; the BUU calculations (with an incompressibility modulus $K=215$ MeV) agree with the measured cross sections, except for the smallest polar angle where the BUU calculations do not treat neutron evaporation.

The La-La data at 400*A* MeV permitted us to extend our ealier studies of the maximum azimuthal anisotropy ratio as a probe of the nuclear equation of state, and to conclude that the maximum azimuthal anisotropy ratio is insensitive to the beam energy from 250 to 400 A MeV for the La-La system. The uncertainties in the measurement of the maximum azimuthal anisotropy ratio are about 15% which do not allow us to investigate its dependence on the mass of the projectile-target system. BUU calculations confirm the lack of sensitivity of the maximum azimuthal anisotropy ratio to the mass of the colliding system and to the beam energy. BUU calculations suggest also that the maximum azimuthal anisotropy ratio is insensitive to the incompressibility modulus K in the nuclear equation of state.

The flow of neutrons was extracted from the slope at midrapidity of the curve of the average in-plane momentum verses the neutron center-of-mass rapidity. The flow of neutrons emitted in La-La collisions at 250 and 400 A MeV increases with beam energy. BUU calculations with an incompressibility modulus $K=215$ MeV for free neutrons agree generally with the data.

We observed the preferential emission of neutrons in a direction perpendicular to the reaction plane in three systems [viz. 400 and 250 A MeV La-La, and 400*A* MeV Nb-Nb]. This component of collective flow, observed first for charged particles is known as out-of-plane squeeze out. BUU calculations of out-of-plane squeeze out of free neutrons are insensitive to the incompressibility modulus K for values of 150, 215, and 380 MeV. After correcting the experimental results to zero dispersion, the observed squeeze out of neutrons is significantly stronger than that from BUU theory.

ACKNOWLEDGMENTS

This work was supported in part by the National Science Foundation under Grant Nos. PHY-91-07064, PHY-88-02392, and PHY-86-11210, the U.S. Department of Energy under Grant Nos. DE-FG89ER40531 and DE-AC03-76SF00098, and the Natural Sciences and Engineering Research Council of Canada and by the Fonds FCAR of the Quebec Government.

[1] L. P. Csernai and J. J. Kapusta, Phys. Rep. **131**, 223 (1986).
[2] R. B. Clare and D. Strottman, Phys. Rep. **141**, 177 (1986).
[3] H. Stöcker and W. Greiner, Phys. Rep. **137**, 277 (1986).
[4] R. Stock, Phys. Rep. **135**, 116 (1986).
[5] D. Beavis, S. Y. Fung, W. Gorn, D. Keane, Y. M. Liu, R. T. Poe, G. VanDalen, and M. Vient, Phys. Rev. Lett. **54**, 1652 (1985).
[6] D. Beavis, S. Y. Chu, S. Y. Fung, W. Gorn, D. Keane, Y. M. Liu, G. VanDalen, and M. Vient, Phys. Rev. C **33**, 1113 (1986).
[7] P. Danielewicz and G. Odyniec, Phys. Lett. **157B**, 146 (1985).
[8] K. G. R. Doss *et al.*, Phys. Rev. C **32**, 116 (1985).
[9] K. G. R. Doss *et al.*, Phys. Rev. Lett. **57**, 302 (1986).
[10] H. Å. Gustafsson *et al.*, Phys. Rev. Lett. **52**, 1590 (1984).
[11] H. H. Gutbrod, K. H. Kampert, B. W. Kolb, A. M. Poskanzer, H. G. Ritter, and H. R. Schmidt, Phys. Lett. B **216**, 267 (1989).
[12] H. H. Gutbrod, K. H. Kampert, B. Kolb, A. M. Poskanzer, H. G. Ritter, R. Schicker, and H. R. Schmidt, Phys. Rev. C **42**, 640 (1990).
[13] H. G. Ritter *et al.*, Nucl. Phys. **A447**, 3c (1985).
[14] Y. Leifels *et al.*, Phys. Rev. Lett. **71**, 963 (1993).
[15] K. G. R. Doss *et al.*, Phys. Rev. Lett. **59**, 2720 (1987).
[16] A. Baden *et al.*, Nucl. Instrum. Methods Phys. Res. **203**, 189 (1982).
[17] D. Keane, S. Y. Chu, S. Y. Fung, Y. M. Liu, L. J. Qiao, G. VanDalen, M. Vient, and S. Wang, Phys. Rev. C **37**, 1447 (1988).
[18] W. M. Zhang *et al.*, Phys. Rev. C **52**, 2643 (1995).
[19] M. Elaasar *et al.*, Phys. Rev. C **49**, R10 (1994).
[20] M. Elaasar, doctoral dissertation, Kent State University, 1993.
[21] R. Madey *et al.*, Nucl. Phys. **A553**, 779c (1993).
[22] G. M. Welke, M. Prakash, T. T. S. Kuo, S. Das Gupta, and C. Gale, Phys. Rev. C **38**, 2101 (1988).
[23] A. R. Baldwin and R. Madey, Nucl. Instrum. Methods Phys. Res. **171**, 149 (1980).

[24] R. A. Cecil, B. D. Anderson, and R. Madey, Nucl. Instrum. Methods Phys. Res. **161**, 439 (1979).
[25] R. Madey, F. M. Waterman, A. R. Baldwin, J. N. Knudson, J. D. Carlson, and J. Rapaport, Nucl. Instrum. Methods Phys. Res. **151**, 445 (1978).
[26] R. Madey *et al.*, Nucl. Instrum. Methods Phys. Res. **214**, 401 (1983).
[27] C. Cavata, M. Demoulins, J. Gosset, M. C. Lemaire, D. L'Hôte, J. Poitou, and O. Vallette, Phys. Rev. C **42**, 640 (1990).
[28] G. Fai, W. M. Zhang, and M. Gyulassy, Phys. Rev. C **36**, 597 (1987).
[29] W. M. Zhang *et al.*, Phys. Rev. C **42**, R491 (1990).
[30] M. Gyulassy, K. A. Frankel, and H. Stöcker, Phys. Lett. **110B**, 185 (1982).
[31] J. J. Molitoris, D. Hahn, and H. Stöcker, Nucl. Phys. **A447**, 13c (1985).
[32] Ch. Hartnack, J. Aichelin, H. Stöker, and W. Greiner, Phys. Lett. B **336**, 131 (1994).
[33] R. Madey, J. Varga, A. R. Baldwin, B. D. Anderson, R. A. Cecil, G. Fai, P. C. Tandy, J. W. Watson, and G. D. Westfall, Phys. Rev. Lett. **55**, 1453 (1985).
[34] R. Madey *et al.*, Phys. Rev. C **42**, 1068 (1990).
[35] G. F. Bertsch and S. Das Gupta, Phys. Rep. **160**, 189 (1988).
[36] J. Aichelin and G. F. Bertsch, Phys. Rev. C **31**, 1730 (1985).
[37] J. Zhang and C. Gale, Phys. Rev. C **51**, 1425 (1995).
[38] C. Gale, G. M. Welke, M. Prakash, S. J. Lee, and S. Das Gupta, Phys. Rev. C **41**, 1545 (1990).